Cardiovascular Diabetology

RESEARCH

Open Access

BDH1 overexpression alleviates diabetic cardiomyopathy through inhibiting H3K9bhb-mediated transcriptional activation of LCN2

Bu-tuo Xu[1,2†], Sheng-rong Wan[3,4,5†], Qi Wu[6,7†], Yi-hang Xing[1,3], Yan-qiu He[1,3], Wei Huang[1,3], Yang Long[3,4], Chun-xiang Zhang[3*], Yong Xu[1,3,5*] and Zong-zhe Jiang[1,3,5,8*]

Abstract

Background Diabetic cardiomyopathy (DbCM) is one of the common complications in diabetic patients, but there is no effective treatment for it up to now. Ketone bodies such as β-OHB have been widely reported to be beneficial for metabolic diseases including various diabetic complications. However, the role of ketone metabolism, especially the relevant enzymes, in the pathogenesis of DbCM is poorly understood.

Methods and results In this study, we firstly observed BDH1, the rate-limiting enzyme of ketone metabolism, was markedly diminished in cardiac tissues from *db/db* mice and diabetic patients, as well as in H9C2 cells treated with palmitic acid. Genetic deletion of BDH1 aggravated, whereas AAV-mediated BDH1 overexpression attenuated, the diastolic dysfunction and pathogenic progression including apoptosis, fibrosis and inflammation of hearts from *db/db* mice. Likewise, BDH1 knockdown promoted, whereas BDH1 overexpression reversed, the palmitic acid-induced lipotoxicity in H9C2 cells. Transcriptome analysis revealed that BDH1 negatively regulated LCN2 expression and LCN2 overexpression largely abrogated BDH1 overexpression-mediated myocardial protection in vitro and in vivo. Mechanistically, BDH1 overexpression reprogrammed ketone metabolism with increased AcAc and decreased β-OHB, thereby resulting in decreased β-hydroxybutyrylation of H3K9 on promoter region of LCN2, which repressed transcription of LCN2 and ultimately inhibited NF-κB activity through weakening interaction between NF-κB and RPS3. Furthermore, oral administration of β-hydroxybutyrylation inhibitor A485 to diabetic mice mitigated the cardiac injury concurrently with decreased expression of LCN2.

Conclusion Our results uncovered a novel mechanism whereby myocardial BDH1 ameliorates DbCM via epigenetic regulation of *LCN2,* which highlights the potential of BDH1/LCN2–based therapeutics in DbCM.

Keywords Diabetic cardiomyopathy, BDH1, LCN2, Lipotoxicity, β-Hydroxybutyrylation

†Bu-tuo Xu, Sheng-rong Wan and Qi Wu contributed equally to this work.

*Correspondence:
Chun-xiang Zhang
zhangchx999@163.com
Yong Xu
xywyll@aliyun.com
Zong-zhe Jiang
jiangzongzhe555@126.com

Full list of author information is available at the end of the article

Background

Diabetes is a chronic metabolic disease that poses a serious threat to human health, and according to the International Diabetes Federation (IDF), the global prevalence of diabetes in 20–79 year olds is estimated to be 10.5% (536.6 million people) in 2021, rising to 12.2% (783.2 million people) in 2045 [1]. Type 2 diabetes is the most common type of diabetes, accounting for over 90% of all diabetes worldwide, and cardiovascular complications are responsible for more than half of type 2 diabetes mortality [2, 3]. As one of the cardiovascular complications, diabetic cardiomyopathy (DbCM) is a diabetes-induced pathophysiological condition in which heart failure occurs in the absence of hypertension and coronary artery disease, and is characterized by left ventricular hypertrophy and reduced diastolic function, with or without concurrent systolic dysfunction [4]. To date, the underlying mechanism of DbCM has not been completely elucidated, the main benefits of intensive glycemic control are non-cardiovascular, and existing therapies are based on the treatment of heart failure [5, 6]. Therefore, it's imperative to clarify the pathogenesis of DbCM and explore accurate therapeutic targets for the treatment of DbCM.

Ketone bodies, including beta-hydroxybutyrate (βOHB), acetoacetate (AcAc), and acetone, serve as energy fuels for extrahepatic tissues such as brain, heart, or skeletal muscle [7]. In the fed state, ketone bodies provide about 5% of the body's total energy requirements, rising to about 20% in fasting [8]. It has been proven that the inhibitor of sodium-glucose cotransporters 2 (SGLT2i) increase circulating ketone body concentrations in human and mice [9, 10], and this is partly why it has an impressive benefit on cardiovascular and all-cause mortality [11, 12]. Though the application of ketogenic diets and ketone bodies as therapeutic tools has arisen in diabetes and its related complications [13–15], the increased risk of ketoacidosis can't be ignored [16]. Furthermore, the effects of ketone body therapy on improving diabetic cardiomyopathy in vivo have been variable [17, 18]. β-hydroxybutyrate dehydrogenase 1 (BDH1), the rate-limiting enzyme of ketone body metabolism, catalyzes the reversible reaction of AcAc to βOHB [7] and *Bdh1* knockout mice have lower total ketone bodies than WT mice, especially after fasting [19]. Cardiac-specific overexpression of Bdh1 can significantly ameliorate TAC-induced heart failure by inhibiting oxidative stress [20]. In our previous study on MAFLD, Bdh1-mediated βOHB metabolism inhibits oxidative stress by activating Nrf2 through up-regulation of fumarate production [21]. However, the role of Bdh1-mediated ketone body metabolism in the pathogenesis of DbCM is still unknown.

In addition to being a modulator of anti-oxidative stress, βOHB is an epigenetic modifier of histone lysine β-hydroxybutyrylation [22]. It has been reported that exogenous βOHB antagonize aortic endothelial injury by causing marked elevation of H3K9bhb in diabetic rat [23]. Similarly, βOHB treatment up-regulates the level of H3K9bhb in the promoter region of the MMP-2 and improves diabetic glomerulosclerosis [24]. All of the above reports suggest that the level of H3K9bhb is related to the concentration of βOHB. Moreover, BDH1 deficiency potentiates propagation of hepatocellular carcinoma stem cells by promoting H3K9bhb through induction of βOHB accumulation [25]. However, the role of BDH1-mediated histone β-hydroxybutyrylation in the pathogenesis of DbCM is still unclear.

In the present study, we report that Bdh1 deficiency contributes to the pathogenesis of DbCM in vivo and palmitic acid-induced lipotoxicity in vitro. We further identify LCN2 as a key downstream effector of BDH1. Mechanistically, we demonstrate that BDH1 reduction induces ketone metabolic reprogramming with βOHB accumulation and increases the H3K9bhb enrichment on the promoter of *Lcn2*, which leads to transcriptional activation and subsequently activates NF-κB through enhancing the interaction between NF-κB and RPS3. Notably, treatment with the histone β-hydroxybutyrylation inhibitor A485 alleviates the progression of DbCM. Taken together, our findings reveal a promising new therapy for DbCM via targeting Bdh1-mediated ketone body metabolism and a novel mechanism by which metabolic reprogramming and epigenetic modification co-regulates the progression of DbCM.

Methods

Animals

Five-week-old male *db/m* and *db/db* mice were purchased from GemPharmatech Co., Ltd. (Nanjing, China). *Bdh1* knockout *(Bdh1−/−)* mice were purchased from Cyagen Biosciences Inc. (Suzhou, China). *db/m* and *Bdh1−/−* mice were crossed to generate *db/db; Bdh1−/−* mice. To overexpress BDH1 or LCN2 in vivo, 100 μL AAV9-*Bdh1* (3.40E+12 vg/mL) or AAV9-*Lcn2* (2.10E + 12vg/mL) and the corresponding control AAV per mouse were injected into *db/m* or *db/db* mice via the caudal vein. All the AAV used in this study were purchased from Syngentech Co. LTD (Beijing, China). Body weight and blood glucose were recorded weekly. All animal experiments were performed under the following conditions: room temperature 23 ± 1 ℃, relative humidity 60% ± 10%, and an alternating 12 h light–dark cycle in individually ventilated cages. Animal experiments were approved by the Institutional Animals Ethics Committees of Southwest Medical University (20220225-014).

Echocardiography

Echocardiograms were performed by a VEVO 3100 ultrasound (VisualSonics, Canada). Mice were anaesthetized with 1.5–2% isoflurane and placed on a temperature-controlled heating pad with a consistent temperature. Cardiac function parameters were collected, including ejection fraction (EF), fractional shortening (FS), Peak E/A ratio et al. The visualization and analysis of the above data were performed with the VEVO 3100 software.

Human heart samples

Human heart samples used in this study were obtained from autopsy in pathology department according to whether there was a clear history of diabetes before death. All procedures that involved human samples were approved by the Affiliated Hospital of Southwest Medical University Ethics Committee (KY2023221).

Cell culture

Rat myocardial cells (H9C2) were subcloned from a cloned cell line of BD1X rat embryonic heart tissue, provided by the Institute of Myocardial Electrophysiology of Southwest Medical University in Luzhou, China. H9C2 cells were cultured at 37 ℃ with 5% CO_2 until 60–70% confluence. Then, cells were exposed to normal control (vehicle 40 μM BSA) and palmitic acid (PA; 150 μM, Sigma-Aldrich, Saint Louis, MO, USA) for 24 h and treated with normal glucose (NG; 5.5 mM) and high glucose (HG; 40 mM) for 48 h. PA was prepared as previously described [21, 26].

RNA-seq study and analysis

Total RNA from cardiac tissues was extracted separately using Trizol Reagent (Invitrogen, Carlsbad, CA, USA) following the manufacturer's procedure. All purified libraries were sequenced using an Illumina NovaSeq 6000 (LC Sciences, CA, USA) at Shanghai Majorbio BioPharm Technology Co., Ltd., (Shanghai, China). Gene expression was normalized to the number method of fragments per kilobase per million reads. The resulting *P*-values were adjusted following the Benjamini and Hochberg method to regulate the false discovery rate. DEGs were identified based on an adjusted *P*-values of < 0.05 and $|\log2(\text{fold change})| \geqq 1.5$ or 2.

Histological assay

The cardiac tissues were fixed in 4% paraformaldehyde for 24 h, embedded in paraffin and sectioned at 4-μm thickness. The sections were stained by the hematoxylin–eosin (H&E) or Masson-trichrome methods for light microscopic analysis and morphometry.

Immunostaining

For immunohistochemistry staining, 4-μm-thick paraffin sections were dewaxing hydration and stained with primary antibodies against BDH1 (1:300, ab193156, Abcam, UK), IL-18 (1:200, AF7266, Beyotime, China), IL-1β (1:200, AF7209, Beyotime, China). The sections were stained with biotin-labeled goat anti-rabbit IgG or biotin-labeled anti-mouse IgG and then treated with the Horseradish enzyme labeled opaltin of Streptomyces (Beijing ZSGB Biological Technology CO., LTD. China). Each photograph of the stained sections was scanned using a light microscope.

For immunofluorescence staining, sections of heart tissues or H9C2 cells were incubated overnight at 4℃ with antibodies against LCN2 (1:100, AF7362, Beyotime, China), NF-κB p65 (1:100, #8242 CST, USA), Phospho-NF-κB p65 (1:100, #3033 CST, USA), H3K9bhb (1:100, PTM-1250RM, PTM, China). Then, the cells were incubated with Alexa Fluor 488/555 fluorescent dye-conjugated secondary antibodies for 1 h in the dark. DAPI (Abcam, UK) was used for nuclear staining. A fluorescence microscope (Leica, Germany) was used for observation.

TUNEL assay

TUNEL staining for the cardiac paraffin sections were performed according to the TUNEL Kit protocol (Vazyme, China).

siRNA and cDNA transfection

The BDH1-overexpressed plasmid (pCMV3-Flag-BDH1), LCN2-overexpressed plasmid (pCMV3-Flag-LCN2) and the Vector plasmid (pCMV3) were purchased from Sino Biological Inc. (Beijing, China). The siRNAs targeted for *Bdh1* or *Lcn2* were purchased from HippoBio (Huzhou, China). si*Bdh1,* si*Lcn2,* Flag-BDH1, Flag-LCN2 and the corresponding control siRNA or Vector plasmid were transfected into H9C2 cells with NanoTrans 20™ (Syngentech Co. LTD. Beijing, China).

Measurement of AcAc and βOHB

The AcAc and βOHB content in H9C2 cells or heart tissues was measured by acetoacetate ELISA Kit and beta-hydroxybutyrate ELISA Kit (J&L Biotech, Shanghai, China) according to the manufacturer's instructions.

qRT-PCR analysis

Total RNA of cardiac tissue or H9C2 cells were extracted with the Trizol (Invitrogen, USA). HiScript III All-in-one RT SuperMix (R333-01, Vazyme) was used for reverse transcription reaction and ChamQ Universal SYBR qPCR Master Mix (Q711-02, Vazyme) was used for qRT-PCR. The qRT-PCR was performed with Analytikjena qTOWER 3G real-time PCR system (JENA, Germany)

according to the manufacturer's instructions. GAPDH was used as an internal reference gene to normalize target gene expression. All the samples were used in triplicate. The $2^{-\triangle\triangle Ct}$ method was used to calculate the relative gene expression in comparison with the reference gene.

Immunoprecipitation and western blot analysis

For immunoprecipitation (IP), H9C2 cells with indicated treatment were suspended in lysis buffer (P0013J, Beyotime, China), supplemented with 1 mM PMSF and 1 mM protease inhibitor cocktail (P1005, Beyotime, China). Lysates were centrifuged at 13,000 g for 10 min, and the supernatant was added to 2 μL indicated antibodies and 100 μL protein A agarose beads (Invitrogen, USA) to incubate for 4 h at 4 °C. Afterward, protein A beads were washed by 250 mM NaCl 4 times. For western blot, total proteins of heart tissue and H9C2 cells were extracted with RIPA extraction buffer (Beyotime Biotechnology, China). Then the protein samples were separated by sodium dodecyl sulfate–polyacrylamide gel electrophoresis (SDS-PAGE) and transferred into a PVDF membrane (Millipore, USA). The membranes were incubated with 5% BSA to block other contaminants, and then with primary antibodies.

Immunoblotting was performed using anti-BDH1 antibody (ab193156, Abcam, UK), anti-Tubulin antibody (AF5012, Beyotime, China), anti-GAPDH antibody (AG8015, Beyotime, China), anti-β actin antibody (AF5003, Beyotime, China), anti-IL-18 antibody (AF7266, Beyotime, China), anti-IL-1β antibody (AF7209, Beyotime, China), anti-Caspase-3 antibody (AF1213, Beyotime, China), anti-LCN2 antibody (AF7362, Beyotime, China), anti-Flag antibody (AF519, Beyotime, China), anti- NF-κB p65 antibody (#8242 CST, USA), anti-Phospho-NF-κB p65 antibody (#3033 CST, USA), anti-RPS3 antibody (AF1045, Beyotime, China), anti-H3 antibody (#4499, CST, USA), anti-H3K9bhb antibody (PTM-1250RM, PTM, China) and anti-H3K9ac antibody (PTM-156, PTM, China).

Chromatin immunoprecipitation assay

The Chromatin Immunoprecipitation Kit (Cat. No. 50034, Absin, China) was utilized to perform chromatin immunoprecipitation (ChIP) assays following the manufacturer's protocol. In brief, nucleic acids and DNA-binding proteins were crosslinked in cellular chromatin samples. A total of 10^7 cells were used, and the chromatin was sonicated to obtain fragments ranging from 200 to 500 bp in ChIP dilution buffer. The resulting DNA fragments were immunoprecipitated using an anti-H3K9bhb antibody (diluted 1:50) or a negative control IgG antibody (1:50) in dilution buffer and incubated overnight at 4 °C. Immunomagnetic beads were then used to enrich the antibody-bound complexes. Following enrichment, the crosslinks were reversed by incubating the complexes at 65 °C for 5 h in elution buffer to release the DNA fragments. DNA was subsequently isolated from the eluate. Real-time quantitative PCR (qRT-PCR) was conducted using primers specifically designed to target the predicted H3K9bhb binding site on the *Lcn2* promoters.

Isolation and culture of primary cardiomyocytes

The Mouse Primary Cardiomyocyte Isolation Kit (Cat. No. 88281) was purchased from Thermo Fisher Scientific. Following the enclosed instructions, we performed the isolation procedure as described below. Firstly, freshly dissected neonatal mouse hearts were cut into small pieces of approximately 1–3 mm^3 in size and thoroughly washed with HBSS. To ensure complete enzymatic digestion, recombinant cardiomyocyte isolation enzymes 1 (containing papain) and 2 (containing collagenase) were added. After confirming digestion, we proceeded with cell yield and viability assessments. Finally, the isolated cardiomyocytes were cultured in a medium consisting of DMEM, supplemented with 10% fetal bovine serum (FBS), 1% penicillin/streptomycin (P/S), and 1‰ cardiomyocyte growth supplement. The cells were incubated at 37 °C in a humidified incubator with 5% CO2.

Statistical analysis

Data are expressed as the means ± standard deviation (SD). The student's t-test was employed for comparisons between two groups. For multiple comparisons, one-way ANOVA was used with Tukey's test. Differences were evaluated using GraphPad Prism9. $P < 0.05$ was considered statistically significant. The statistical significance was $^{*}p < 0.05$, $^{**}0.001 < p < 0.01$; $^{***}P < 0.001$.

Results

BDH1 expression was reduced in diabetic hearts and palmitic acid (PA)-treated H9C2 cells

Given that Type 2 diabetes (T2DM) is the most common type of diabetes and cardiovascular complications are responsible for more than half of T2DM mortality [2, 3], here we employed *db/db* mice, a classic genetic model of T2DM, to establish DbCM mouse model (Fig. S1A-B). Hearts from *db/db* mice with high fat diet feeding for 12 weeks showed decreased diastolic function, increased fibrosis and inflammation, but showed no change in systolic function (Fig. 1A–D; Fig. S1C-D), which was consistent with the fact that diabetes is a strong risk factor for heart failure with preserved ejection fraction (HFpEF). We next performed RNA-seq with cardiac tissues from these mouse models and observed that BDH1, one of the rate-limiting enzymes of ketone metabolism, ranked ahead in the down-regulated differentially expressed

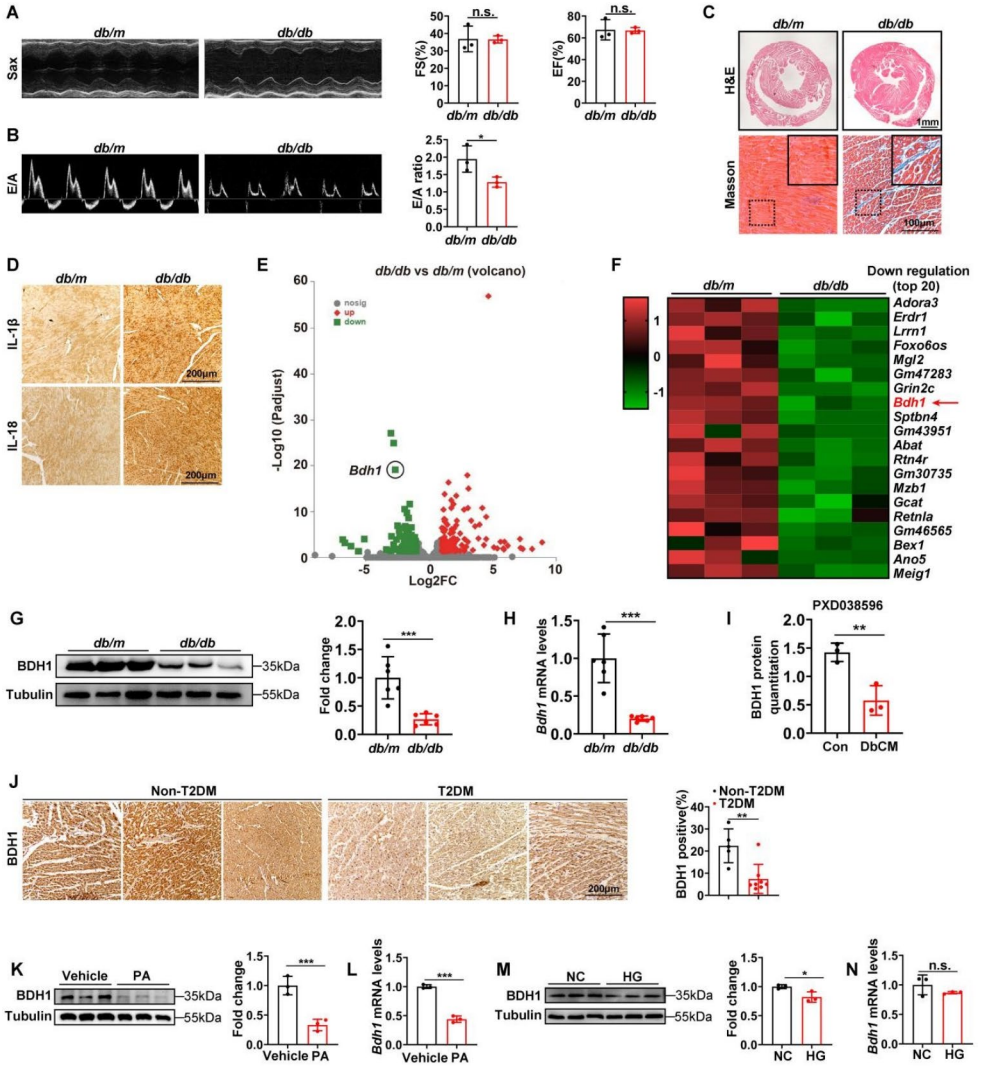

Fig. 1 BDH1 expression was down-regulated in diabetic hearts and palmitic acid (PA)-treated H9C2 cells. **A** Representative left ventricular M-mode echocardiographic tracings in short-axis view, percentage of left ventricular ejection fraction (EF) and fractional shortening (FS) in *db/m* and *db/db* mice. **B** Representative pulsed-wave Doppler tracings and ratio between mitral E wave and A wave (E/A) in *db/m* and *db/db* mice. **C**, **D** Representative images of H&E, Masson staining and immunohistochemistry staining of inflammatory factors for heart sections. Bars: 1 mm in H&E; 100 μm in Masson staining; 200 μm in D. **E**, **F** Volcano plot (**E**) and heat map (**F**) of differentially expressed genes from RNA-seq analysis of *db/m* and *db/db* heart tissues. n = 3 mice per group in **A**–**F**. **G**, **H** Western blot and qRT-PCR analysis showing BDH1 expression in the cardiac tissues from *db/m* and *db/db* mice. n = 6 mice per group in G-H. **I** The protein levels of BDH1 in the cardiac tissues of diabetic rats based on the PXD038596 dataset. **J** Representative immunohistochemistry staining and quantification of BDH1 expression in heart sections from diabetic patients (n = 8) and healthy controls (n = 5). Bar: 200 μm. **K**, **M** Representative immunoblotting images and quantification of BDH1 protein level in the H9C2 cells in the presence or absence of PA (**K**) or HG (**M**). **L**, **N** qRT-PCR analysis showing BDH1 mRNA expression in the H9C2 cells treated with PA (**K**) or HG (**M**). PA: palmitic acid; HG: high glucose. n = 3 repeated experiments in **K**–**N**. Values are presented as mean ± SD. **P < 0.05; **P < 0.01; ***P < 0.001*

genes (Fig. 1E, F), which was further confirmed by protein detection with western blot and mRNA detection with real time PCR (Fig. 1G, H). Besides, we also screened the available databases and found that BDH1 protein level was significantly down-regulated in the hearts from diabetic rats in a proteomics data sheet PXD038596 (Fig. 1I). We next examined the expression of BDH1 in the heart tissues of patients with T2DM. As shown in Fig. 1J, BDH1 expression was significantly reduced in cardiac samples from diabetic patients compared with that in normal people, whereas the expression of cardiac marker cTnT showed no changes (Fig. S1E).

To determine the possible reason for BDH1 reduction in diabetes, we used H9C2 cells to establish lipotoxicity and glucotoxicity cell models with stimulation of palmitic acid (Fig. S1F-H) or high glucose, which are common stimuli implicated in diabetes. Interestingly, palmitic acid stimulation induced obvious reduction of BDH1 either in protein or mRNA levels (Fig. 1K, L), but high glucose led to minor reduction of BDH1 in protein level and

no change in mRNA level (Fig. 1M, N). Taken together, these results indicate that the reduction of cardiac BDH1 is a prominent phenomenon under T2DM conditions, which might contribute to the pathogenesis of diabetic cardiomyopathy.

BDH1 deficiency aggravates diabetes-induced cardiac dysfunction in vivo and palmitic acid-induced cardiomyocyte injury in vitro

Given the dramatic changes of BDH1 expression observed in diabetic heart tissues and palmitic acid-stimulated cardiomyocytes, we next crossed *db/m* mice with *Bdh1−/−* mice to generate BDH1-deleted *db/db* mice (hereafter referred to as *db/db; Bdh1−/−*) to study the role of BDH1 in DbCM (Fig. 2A, B; Fig. S2A). Although *db/db* mice with WT genotype of *Bdh1* (hereafter referred to as *db/db; WT)* showed no changes in systolic function after 12 weeks' HFD feeding, BDH1 knockout led to systolic dysfunction with decreased ejection fraction (EF) and fractional shortening (FS) in *db/db; Bdh1−/−* mice (Fig. 2C). Moreover, compared to *db/m* mice, *db/db; WT* mice exhibited diastolic dysfunction with decreased *E/A* ratio, which was exacerbated by BDH1 deletion in *db/db; Bdh1−/−* mice (Fig. 2D). As expected, pathological analysis showed elevated lipotoxicity, fibrosis, apoptosis and inflammation in cardiac tissues from *db/db; WT* mice, which was aggravated in that from *db/db; Bdh1−/−* mice (Fig. 2E–G; Fig. S2B, 2F). Notably, BDH1 deletion in *db/m* mice exhibited no effect on cardiac function and pathological phenotype compared to that with WT genotype of *Bdh1* (Fig. 2C–G), which indicates that BDH1 deficiency selectively induces cardiac injury in diabetic condition.

Given that the cardiomyocytes are susceptible to lipid accumulation and lipotoxicity in obesity-related metabolic disease [26] and BDH1 expression was reduced in palmitic acid-treated H9C2 cells (Fig. 1K, L), we wonder whether BDH1 deficiency contributes to lipotoxicity in cardiac cells. To this end, we disturbed BDH1 expression in H9C2 cells with BDH1 siRNA transfection and treated them with vehicle or palmitic acid (Fig. 2H; Fig. S2C). In line with that observed in mouse model, BDH1 knockdown exacerbated inflammation and apoptosis with elevated cleaved IL-18, IL-1β and caspase 3 in H9C2 cells treated by palmitic acid, but exhibited no change in that treated by vehicle (Fig. 2I, J). Real time PCR also confirmed the inflammation activation shown as increased mRNA levels of *IL-1β, IL-6, IL-18* and *TNFα* induced by BDH1 knockdown in H9C2 cells treated by palmitic acid but not vehicle (Fig. 2K). Besides, Tunel assay showed increased apoptotic cells in BDH1-disturbed H9C2 cells with palmitic acid treatment (Fig. 2L; Fig. S2D), as well as the primary cardiomyocytes isolated from fetal *Bdh1−/−* mice (Fig. 2M; Fig. S2E). Collectively, these data indicate that BDH1 deficiency might mediate diabetes-induced cardiac dysfunction through lipotoxicity.

BDH1 overexpression protects against diabetes-induced cardiac dysfunction in vivo and palmitic acid-induced lipotoxicity in vitro

To further confirm the function of cardiac BDH1 in the pathogenesis of DbCM, we next overexpressed BDH1 in 6-week-old *db/m* or *db/db* mice by injection of adenovirus expressing BDH1 (AAV9-*Bdh1*) or GFP (AAV9-Con) followed by HFD feeding for 12 weeks (Fig. 3A, B; Fig. S3A). Compared to *db/m* mice injected with AAV9-Con, *db/db* mice injected with AAV9-Con exhibited no changes in systolic function indexes such as EF and FS, the same as that in *db/db* mice injected with AAV9-*Bdh1* (Fig. 3C). In contrast, *db/db* mice injected with AAV9-Con exhibited impaired diastolic function with decreased *E/A* ratio, which was completely reversed by AAV9-*Bdh1* injection (Fig. 3D). Likewise, pathologic analysis showed elevated lipotoxicity, fibrosis, apoptosis and inflammation in cardiac tissues from *db/db* mice injected with AAV9-Con, which was alleviated in that from *db/db* mice injected with AAV9-*Bdh1*(Fig. 3E–G; Fig. S3B, 3D). To investigate the effect of BDH1 overexpression on lipotoxicity in cardiac cells, we next overexpressed BDH1 in H9C2 cells with Flag-BDH1 transfection and treated them with vehicle or palmitic acid (Fig. 3H; Fig. S3C). As shown in Fig. 3I, BDH1 overexpression reversed palmitic acid-induced elevation of cleaved IL-18 and IL-1β in H9C2 cells, as well as the mRNA levels of *IL-1β, IL-6* and *TNFα* (Fig. 3J). In addition, Tunel assay showed that BDH1 overexpression reversed the palmitic acid-induced apoptosis in H9C2 cells (Fig. 3K), which was consistent with the reduced protein level of cleaved caspase 3 in BDH1-overexpressed H9C2 cells treated by palmitic acid (Fig. 3L). Notably, BDH1 overexpression also increased the serum level of βOHB, but showed no change in serum TC and TG (Fig. S3E-G). These data suggest that BDH1 overexpression attenuates diabetes-induced cardiac dysfunction through protection against lipotoxicity.

BDH1 overexpression attenuates diabetic cardiomyopathy via inhibition of LCN2

To determine the molecular mechanism by which BDH1 overexpression protects against DbCM, we performed RNA sequencing analysis for BDH1-dependent transcriptome profiling in hearts from *db/m* and *db/db* mice injected with AAV9-Con or AAV9-*Bdh1*. Among the differentially expressed genes (DEGs), 8 genes were up-regulated by at least 2 folds in hearts from *db/db* mice injected with AAV9-Con compared with that from db/m mice, meanwhile, were down-regulated by at least 2 folds in hearts from *db/db* mice injected with AAV9-*Bdh1*, including Lipocalin 2 (LCN2) and Interferon regulatory

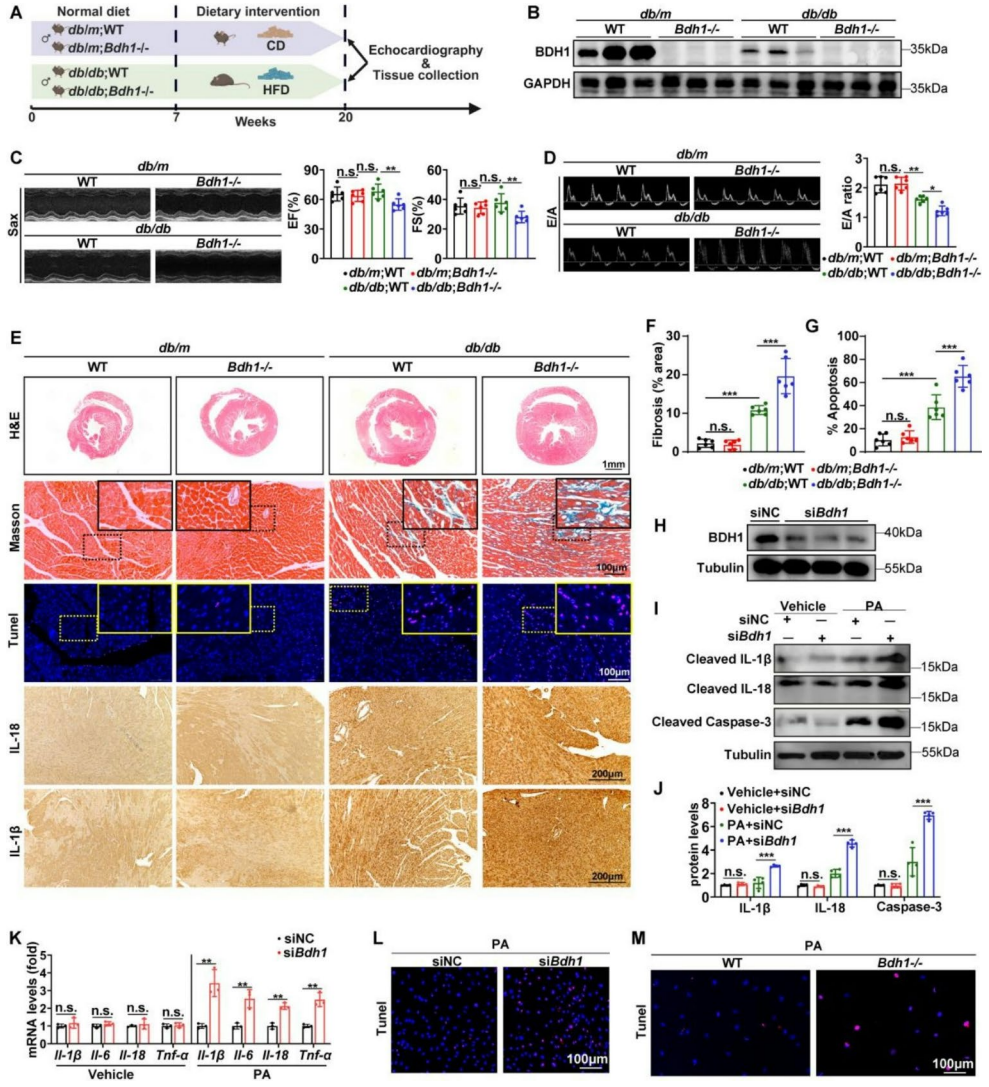

Fig. 2 BDH1 deficiency aggravates diabetes-induced cardiac dysfunction in vivo and palmitic acid-induced cardiomyocyte injury in vitro. Schematic representation of the animal experiment workflow. **B** Representative immunoblotting images of BDH1 protein levels in the cardiac tissues from *db/m*; *WT*, *db/m*; *Bdh1−/−*, *db/db*; *WT* and *db/db*; *Bdh1−/− mice*. **C** Representative left ventricular M-mode echocardiographic tracings, percentage of left ventricular ejection fraction (EF) and fractional shortening (FS) in the indicated mice. **D** Representative pulsed-wave Doppler tracings and ratio between mitral E wave and A wave (E/A) in the indicated mice. **E** Representative images of H&E, Masson staining, Tunel assay and immunohistochemistry staining of inflammatory factors for heart sections from indicated mice. Bars: 1 mm in H&E; 100 μm in Masson staining and Tunel assay; 200 μm in immunohistochemistry staining. **F**, **G** Quantification of fibrosis by assessing the Masson-positive areas (**F**) and apoptosis by counting the Tunel-positive cells (**G**) in the heart sections from indicated mice. n = 6 mice per group. **H** Representative immunoblotting images of BDH1 expression in H9C2 cells transfected with control siRNA (siNC) or *Bdh1* targeted siRNA (si*Bdh1*). **I**, **J** Representative immunoblotting images of inflammatory factors and cleaved caspase 3 in siNC- or si*Bdh1*-transfected H9C2 cells with or without PA treatment. **K** mRNA expression of inflammatory factors in siNC- or si*Bdh1*-transfected H9C2 cells with or without PA treatment. **L**, **M** Tunel assay showing the apoptosis level of siNC- or si*Bdh1*-transfected H9C2 cells (**L**) and primary cardiomyocytes isolated from fetal WT or *Bdh1−/−* mice (**M**) with PA treatment. n = 3 repeated experiments in H-M. Values are presented as mean ± SD. **P < 0.05; **P < 0.01; ***P < 0.001*

factor 7 (IRF7) (Fig. 4A), two inflammatory regulators which have been reported to function in metabolic disease [27, 28]. We next confirmed the expression of these two DEGs in mouse model and cultured H9C2 cells. Notably, real-time PCR showed that both LCN2 and IRF7 were up-regulated in diabetic hearts and palmitic acid-treated H9C2 cells, but only the increased LCN2 expression was reversed by BDH1 overexpression both in diabetic hearts and palmitic acid-treated H9C2 cells (Fig. 4B, C), suggesting LCN2, but not IRF7, as the potential target of BDH1 in protection against lipotoxicity-induced DbCM. In addition, western blots showed increased protein level of LCN2 in *db/db* mice injected with AAV9-Con, which was reversed by AAV9-BDH1 injection (Fig. 4D). In palmitic acid-treated H9C2 cells, BDH1 knockdown increased the protein level of LCN2,

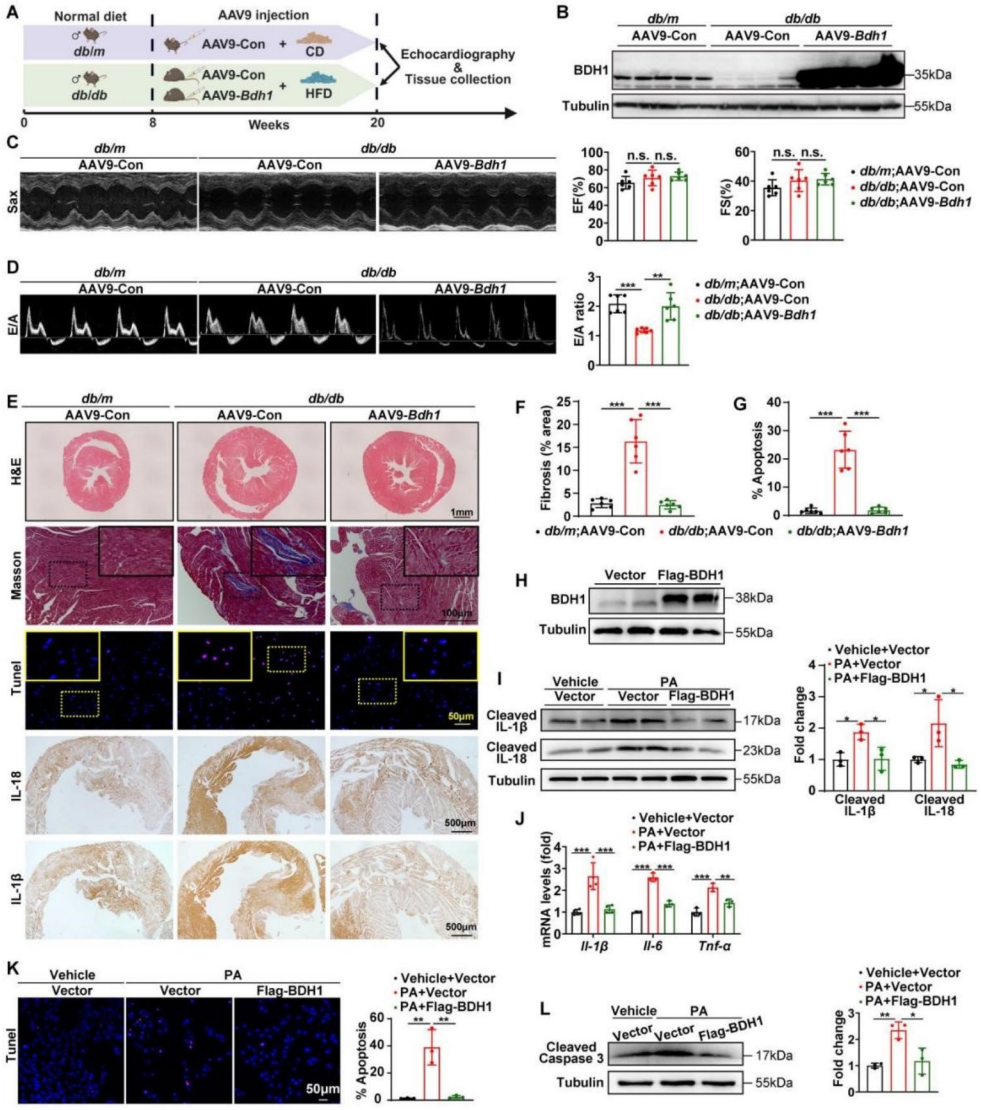

Fig. 3 BDH1 overexpression protects against diabetes-induced cardiac dysfunction in vivo and palmitic acid-induced lipotoxicity in vitro. **A** Schematic representation of the animal experiment workflow. **B** Representative immunoblotting images of BDH1 protein levels in the cardiac tissues from *db/m* or *db/db mice* which were injected with AAV9-Con or AAV9-*Bdh1*. **C** Representative left ventricular M-mode echocardiographic tracings, percentage of left ventricular ejection fraction (EF) and fractional shortening (FS) in the indicated mice. **D** Representative pulsed-wave Doppler tracings and ratio between mitral E wave and A wave (E/A) in the indicated mice. **E** Representative images of H&E, Masson staining, Tunel assay and immunohistochemistry staining of inflammatory factors for heart sections from indicated mice. Bars: 1 mm in H&E; 100 μm in Masson staining; 50 μm in Tunel assay; 200 μm in immunohistochemistry staining. **F**, **G** Quantification of fibrosis by assessing the Masson-positive areas (**F**) and apoptosis by counting the Tunel-positive cells (**G**) in the heart sections from indicated mice. n = 6 mice per group. **H** Representative western blots showing the protein level of BDH1 in H9C2 cells transfected with Vector and Flag-BDH1 plasmids. **I**, **J** Representative western blots and qRT-PCR showing the protein (**I**) and mRNA (**J**) levels of inflammatory factors in Vector- or Flag-BDH1-transfected H9C2 cells with or without PA treatment. **K** Tunel assay showing the apoptosis levels in Vector- or Flag-BDH1-transfected H9C2 cells with or without PA treatment. **L** Representative western blots showing the protein level of cleaved caspase 3 in Vector- or Flag-BDH1-transfected H9C2 cells with or without PA treatment. All results are representative of three independent experiments. Values are presented as mean ± SD. **P < 0.05; **P < 0.01; ***P < 0.001*

as shown in western blot (Fig. 4E) and immunostaining (Fig. 4F). Similarly, in palmitic acid-treated primary cardiomyocytes, BDH1 deletion also increased the LCN2 expression (Fig. 4G). In contrast, overexpression of BDH1 reversed the palmitic acid-induced increase of LCN2 protein level in H9C2 cells, as shown in western blot (Fig. 4H) and immunostaining (Fig. 4I). These data indicate that BDH1 negatively regulates the expression of LCN2.

To further determine whether BDH1 overexpression protects against DbCM through suppression of LCN2, we firstly examined the role of LCN2 in cardiac lipotoxicity. As expected, LCN2 knockdown inhibited, whereas LCN2 overexpression aggravated the palmitic

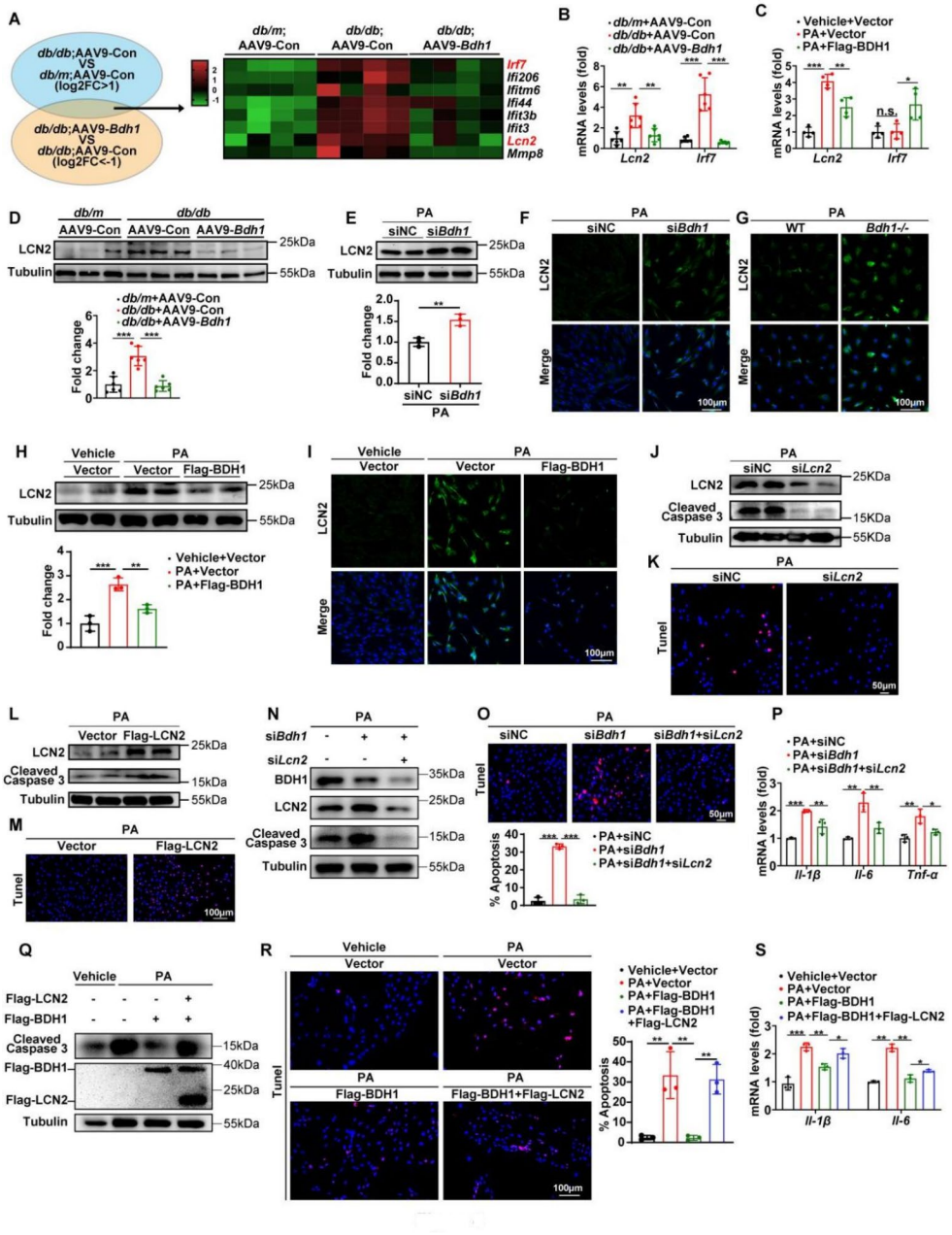

Fig. 4 BDH1 overexpression protects H9C2 cells against PA-induced lipotoxicity via inhibition of LCN2. **A** RNA-seq analysis showing the differentially expressed genes which were up-regulated in AAV9-Con-injected *db/db* mice while down-regulated in AAV9-*Bdh1*-injected *db/db* mice. **B**–**C** qRT-PCR analysis showing the mRNA expression of *Lcn2* and *Irf7* in hearts from *db/m* and *db/db* mice injected with AAV9-Con or AAV9-*Bdh1* (**B**) and H9C2 cells treated with vehicle or PA and transfected with Vector or Flag-BDH1 (**C**). **D**–**I** Representative western blots and immunostaining images showing the protein level of LCN2 in hearts from *db/m* and *db/db* mice injected with AAV9-Con or AAV9-*Bdh1* (**D**), PA-treated H9C2 cells transfected with siNC or si*Bdh1* (**E**–**F**), PA-treated primary cardiomyocytes isolated from fetal WT or *Bdh1*−/− mice (**G**), PA-treated H9C2 cells transfected with Vector or Flag-BDH1 (**H**, **I**). **J**–**M** Representative western blots and Tunel assay showing the apoptosis levels in PA-treated H9C2 cells transfected with siNC or si*Bdh1* (**J**, **K**) and Vector or Flag-BDH1 (**L**, **M**). **N**–**P** Western blotting, Tunel assay and qRT-PCR analysis showing the apoptosis level (**N**, **O**) and mRNA expression of inflammatory factors (**P**) in PA-treated H9C2 cells transfected with siNC, siBdh1 or si*Bdh1* accompanied with si*Lcn2*. **Q**–**S** Western blotting, Tunel assay and qRT-PCR analysis showing the apoptosis level (**Q**, **R**) and mRNA expression of inflammatory factors (**S**) in Vehicle- or PA-treated H9C2 cells transfected with Vector, Flag-BDH1 or Flag-BDH1 accompanied with Flag-LCN2. Bars: 100 μm in F, I, M and R; 50 μm in **K** and **O**. All results are representative of three independent experiments. Values are presented as mean ± SD. **P < 0.05; **P < 0.01; ***P < 0.001*

acid-induced apoptosis in H9C2 cells, as indicated by increased cleaved Caspase 3 levels (Fig. 4J and L; Fig. S4A, 4C) and Tunel signals (Fig. 4K and M; Fig. S4B, 4D). Importantly, LCN2 knockdown eliminated the BDH1 knockdown-induced increase of apoptosis and inflammation with reduced cleaved Caspase 3 (Fig. 4N; Fig. S4F), Tunel signals (Fig. 4O) and mRNA levels of *IL-1β*, *IL-6* and *TNFα* (Fig. 4P), in the cultured H9C2 cells. In contrast, LCN2 overexpression abrogated the BDH1 overexpression-induced inhibition of apoptosis and inflammation with increased cleaved Caspase 3 (Fig. 4Q; Fig. S4E), Tunel signals (Fig. 4R) and mRNA levels of *IL-1β* and *IL-6* (Fig. 4S), indicating that LCN2 functions as a downstream target in the protective effect of BDH1 on lipotoxicity.

To further confirm the role of LCN2 in BDH1-mediated cardioprotective effect in vivo, we co-expressed BDH1 and LCN2 by injecting AAV9-*Bdh1* together with AAV9-*Lcn2* in *db/db* mice (Fig. 5A, B; Fig. S5A). Consistent with that shown previously, there was no significant change in systolic function as indicated by EF and FS values among the four experimental groups (Fig. 5C). Of note, AAV9-*Bdh1* injection alone attenuated the impaired diastolic function as indicated by *E/A* ratio in AAV9-Con-injected

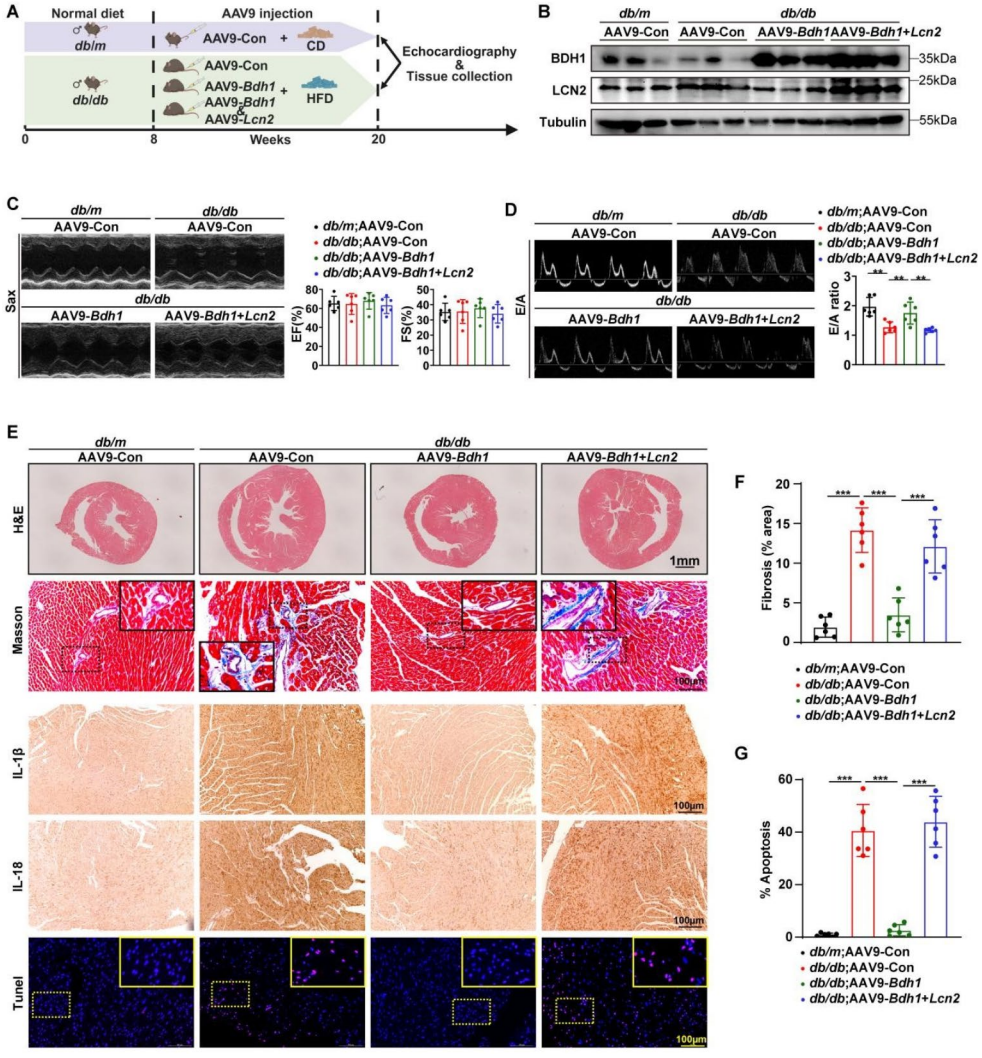

Fig. 5 BDH1 overexpression protects *db/db* mice against cardiac dysfunction via inhibition of LCN2. **A** Schematic representation of the animal experiment workflow. **B** Representative immunoblotting images of BDH1 and LCN2 protein levels in the cardiac tissues from db/m or db/db mice which were injected with AAV9-Con, AAV9-Bdh1 or AAV9-Bdh1 accompanied with AAV9-Lcn2. **C** Representative left ventricular M-mode echocardiographic tracings, percentage of left ventricular ejection fraction (EF) and fractional shortening (FS) in the indicated mice. **D** Representative pulsed-wave Doppler tracings and ratio between mitral E wave and A wave (E/A) in the indicated mice. **E** Representative images of H&E, Masson staining, immunohistochemistry staining of inflammatory factors and Tunel assay for heart sections from indicated mice. Bars: 1 mm in H&E; 100 μm in Masson staining, Tunel assay and immunohistochemistry staining. **F**, **G** Quantification of fibrosis by assessing the Masson-positive areas (**F**) and apoptosis by counting the Tunel-positive cells (**G**) in the heart sections from indicated mice. n = 6 mice per group. All results are representative of three independent experiments. Values are presented as mean ± SD. ***P < 0.01; ***P < 0.001*

db/db mice, which was abolished by co-injection with AAV9-*Bdh1* and AAV9-*Lcn2* (Fig. 5D). Further pathological analysis showed that AAV9-*Bdh1* injection alone reversed the diabetes-induced fibrosis, apoptosis and inflammation in AAV9-Con-injected *db/db* mice, which was abrogated by co-injection with AAV9-*Bdh1* and AAV9-*Lcn2* (Fig. 5E–G; Fig. S5B). Collectively, these data suggest that BDH1 overexpression attenuates diabetic cardiomyopathy via inhibition of LCN2.

BDH1 inhibits LCN2-dependent NF-κB activation

Given that LCN2 has been reported to promote NF-κB activation through interaction with RPS3 [29] and NF-κB activation participates in the development of DbCM [30], we supposed that LCN2 reduction mediates the protective effect of BDH1 on DbCM through inhibiting NF-κB activation. Consistent with the results shown in the previous study [29], immunoprecipitation revealed an obvious interaction between LCN2 and NF-κB in cultured H9C2 cells (Fig. 6A). With co-immunoprecipitation, we observed that palmitic acid treatment enhanced the interaction between LCN2 and NF-κB, which was abolished by BDH1 overexpression (Fig. 6B). Although LCN2 could interact with NF-κB, it was reported that LCN2 activates NF-κB by promoting the interaction between NF-κB and RPS3, an important NF-κB regulator. We thus assessed this regulation in cultured H9C2 cells. As shown in Fig. 6C, overexpression of LCN2 remarkably enhanced the interaction between NF-κB and RPS3, as well as the phosphorylation of NF-κB by which it can enter into nucleus to function. In contrast, LCN2 knockdown weakened the interaction between NF-κB and RPS3, as well as the phosphorylation of NF-κB in the cultured H9C2 cells (Fig. 6D).

We also performed immunostaining of NF-κB to assess its location in BDH1-overexpressed or BDH1 and LCN2-co-expressed H9C2 cells. Notably, BDH1 overexpression reversed the palmitic acid-induced nuclear location of NF-κB, which was abolished by BDH1 and LCN2 co-expression (Fig. 6E). In contrast, BDH1 knockdown promoted the palmitic acid-induced nuclear location of NF-κB, which was abrogated by LCN2 knockdown (Fig. 6F). Furthermore, immunostaining of NF-κB for cardiac sections showed that AAV9-*Bdh1* injection alone reversed the diabetes-induced nuclear location of NF-κB, which was abolished by AAV9-*Bdh1* injection together with AAV9-*Lcn2* (Fig. 6G). Taken together, these results suggest that BDH1 overexpression alleviates DbCM through suppression of LCN2-dependent NF-κB activation (Fig. 6H).

BDH1 down-regulates cardiac βOHB level and represses LCN2 expression via inhibiting H3K9bhb

We further investigated the molecular mechanism by which BDH1 represses the LCN2 expression. Given that BDH1 catalyzes the transformation between βOHB and acetoacetic acid (AcAc), which are the precursors of Kac and Kbhb we supposed that BDH1 might regulate LCN2 expression through metabolites-mediated epigenetic reprogramming. To this end, we firstly examined the effect of BDH1 on the concentrations of βOHB and AcAc. In cardiac tissues from *db/db* mice, the level of βOHB was up-regulated, whereas the level of AcAc was down-regulated compared to that from *db/m* mice, which was consistent with the reduction of BDH1 (Fig. 7A, B). Notably, AAV9-*Bdh1* injection reversed the increase of βOHB and the decrease of AcAc in the cardiac tissues from *db/db* mice injected with AAV9-Con (Fig. 7C, D). However, BDH1 deficiency exacerbated the diabetes-induced reduction of AcAc but not further elevated the level of βOHB as expected (Fig. 7E, F), which might be due to the general BDH1 knockout-induced blockage of hepatic synthesis and serious shortage of serum βOHB (data not shown). In line with what we observed in vivo, palmitic acid treatment led to increased βOHB and decreased AcAc in cultured H9C2 cells (Fig. 7G, H), which was consistent with the palmitic acid-induced reduction of BDH1. Furthermore, BDH1 overexpression reversed the palmitic acid-induced increase of βOHB and decrease of AcAc (Fig. 7I, J), whereas BDH1 knockdown increased βOHB and decreased AcAc in palmitic acid-treated H9C2 cells (Fig. 7K, L), indicating that BDH1 controls the homeostasis of βOHB and AcAc.

We next assessed the effect of BDH1 on H3K9ac and H3K9bhb, which are epigenetic modifications and derived from AcAc and βOHB. As shown in Fig. 7M, palmitic acid increased the level of H3K9bhb in cultured H9C2 cells, which was remarkably reversed by BDH1 overexpression (Fig. S6A). In contrast, the level of H3K9ac was obviously reduced in palmitic acid-treated H9C2 cells, which was reversed by BDH1 overexpression (Fig. 7N; Fig. S6B). Given that the H3K9bhb was reported to repress, while the H3K9ac was reported to promote, the transcription of targeted genes, we concluded that the reduction of H3K9bhb is responsible for the BDH1 overexpression-induced repression of LCN2. Consistent with the notion, we observed that BDH1 knockdown increased the H3K9bhb level in palmitic acid-treated H9C2 cells (Fig. 7O; Fig. S6C) and AAV9-*Bdh1* injection reversed the diabetes-induced increase of H3K9bhb in cardiac tissues from *db/db* mice (Fig. 7P; Fig. S6D). Importantly, we performed chromatin immunoprecipitation combined with real-time PCR (ChIP-PCR) with two primers targeting *Lcn2* promoter region and observed elevated H3K9bhb in promoter region of *Lcn2* in H9C2

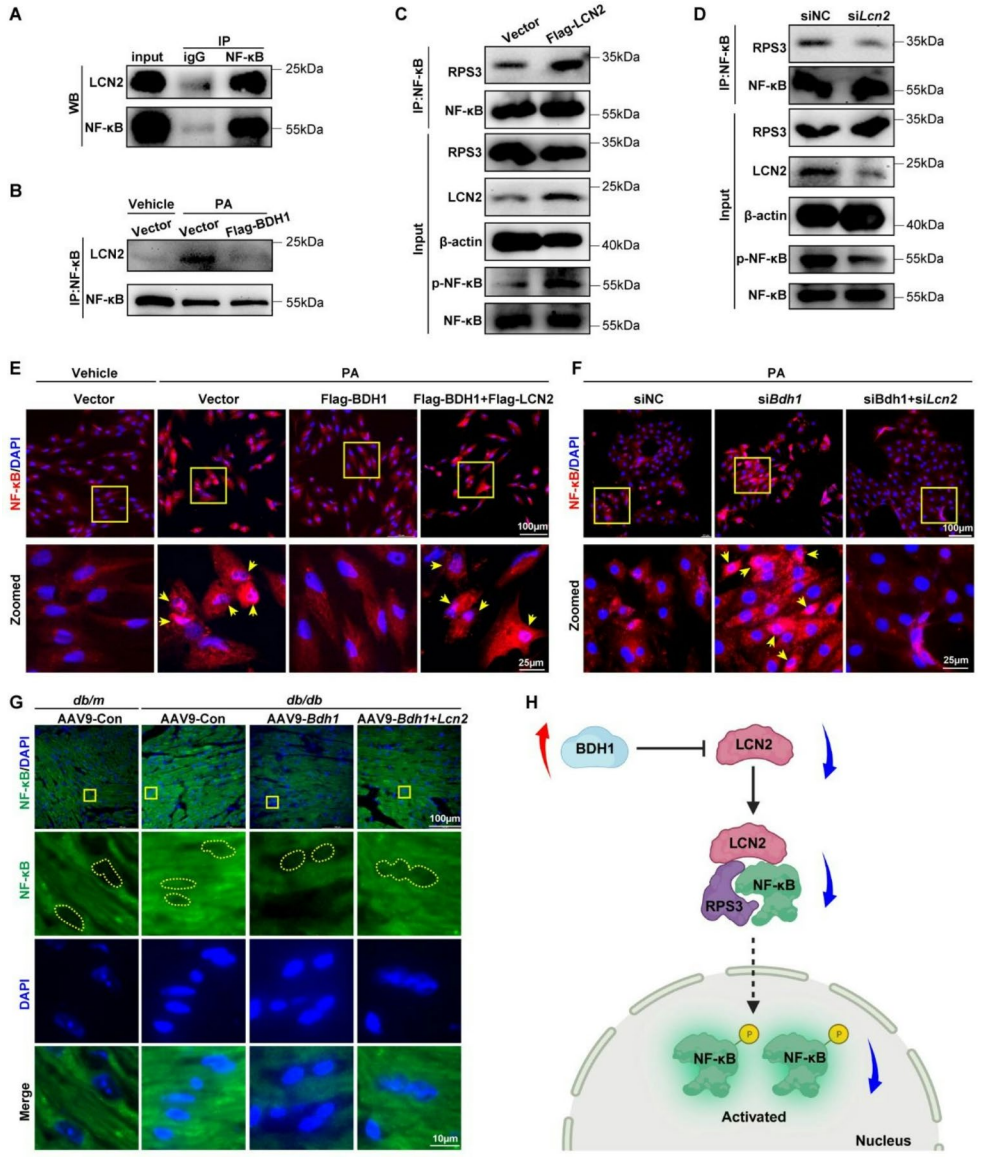

Fig. 6 BDH1 inhibits LCN2-mediated NF-κB activation. **A** Immunoprecipitation and western blot analysis showing the interaction between LCN2 and NF-κB. **B** Immunoprecipitation and western blot analysis showing the interaction between LCN2 and NF-κB in Vector- or Flag-BDH1-transfected H9C2 cells with or without PA treatment. **C**, **D** Immunoprecipitation and western blot analysis showing the interaction between RPS3 and NF-κB and the phosphorylation level of NF-κB in H9C2 cells transfected with Vector or Flag-LCN2 (**C**) and siNC or si*Lcn2* (**D**). **E**, **F** Immunostaing analysis showing the nuclear localization of NF-κB in Vehicle- or PA-treated H9C2 cells transfected with Vector, Flag-BDH1 or Flag-BDH1 accompanied with Flag-LCN2 (**E**) and PA-treated H9C2 cells transfected with siNC, siBdh1 or si*Bdh1* accompanied with si*Lcn2* (**F**). **G** Immunostaining analysis showing the nuclear localization of NF-κB in the cardiac tissues from *db/m* or *db/db mice* which were injected with AAV9-Con, AAV9-*Bdh1* or AAV9-*Bdh1* accompanied with AAV9-*Lcn2*. Bars: 100 μm in the upper panels and 10 μm in the amplified panels. **H** Illustration showing that BDH1 inhibits LCN2-mediated NF-κB activation. All results are representative of three independent experiments

cells transfected with BDH1 siRNA (Fig. 7Q, R). Additionally, palmitic acid led to increased H3K9bhb level in *Lcn2* promoter region, which was reversed by BDH1 overexpression (Fig. 7S). These results indicate that BDH1 overexpression down-regulated the βOHB level and the βOHB dependent H3K9bhb in *Lcn2* promoter region, which ultimately represses the transcription of *Lcn2* (Fig. 7T).

A485 represses LCN2 expression through inhibiting H3K9bhb and attenuates diabetic cardiomyopathy

To further confirm the regulation of H3K9bhb in LCN2 expression, we next employed A485, a strong inhibitor of the acetyltransferase P300 which is known to catalyze lysine β-hydroxybutyrylation, as an inhibitor of H3K9bhb (Fig. 8A). As a result, A485 treatment reversed the palmitic acid-induced increase in both mRNA and protein levels of LCN2, as well as the increased H3K9bhb

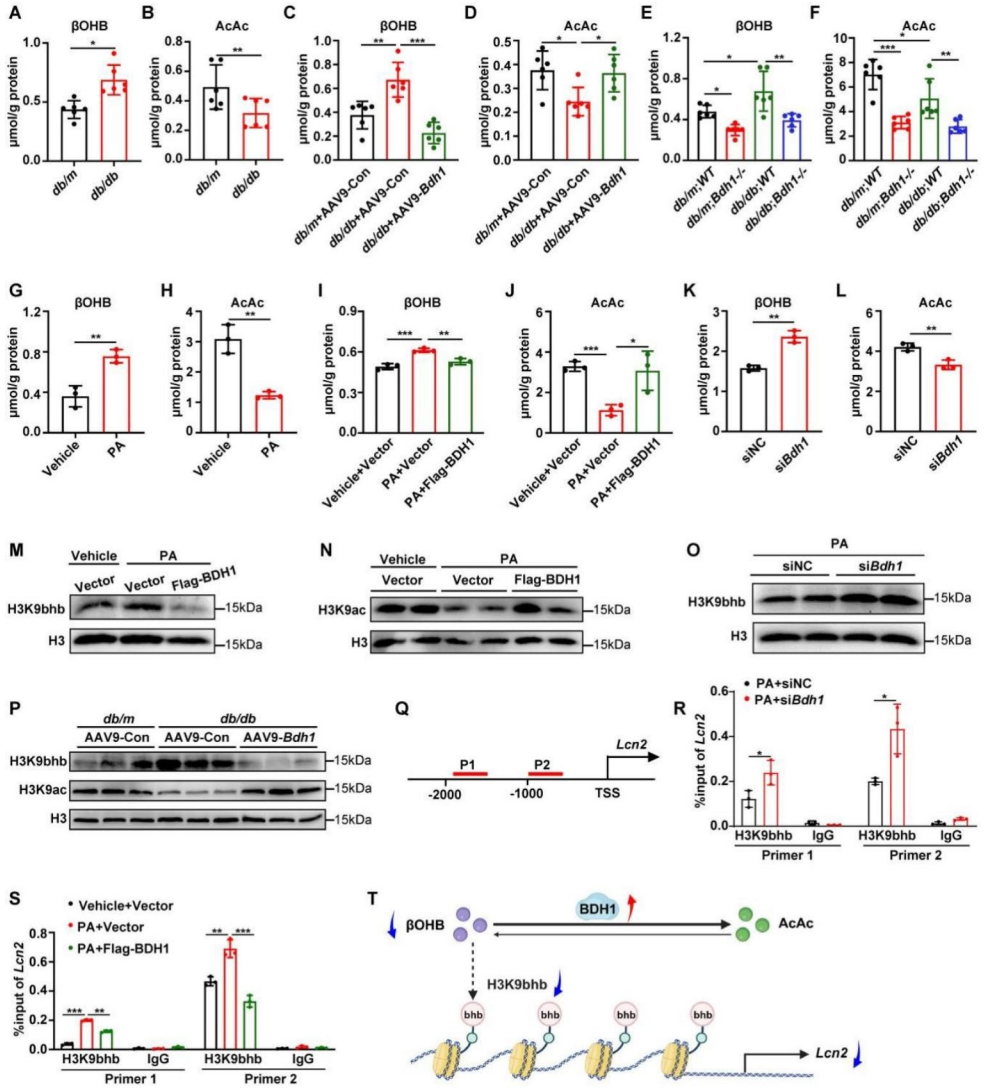

Fig. 7 BDH1 represses LCN2 expression via inhibiting H3K9 β-hydroxybutyrylation. **A**, **B** ELISA analysis showing the concentrations of βOHB and AcAc in cardiac tissues from *db/m* or *db/db* mice. **C**–**F** ELISA analysis showing the concentrations of βOHB and AcAc in cardiac tissues from *db/m or db/db* mice injected with AAV9-Con or AAV9-*Bdh1* (**C**, **D**) and cardiac tissues from *db/m*; *WT*, *db/m*; *Bdh1−/−*, *db/db*; *WT* and *db/db*; *Bdh1−/−* mice (**E**, **F**). **G**, **H** ELISA analysis showing the concentrations of βOHB and AcAc in Vehicle- or PA-treated H9C2 cells. **I**–**L** ELISA analysis showing the concentrations of βOHB and AcAc in Vector- or Flag-BDH1-transfected H9C2 cells with or without PA treatment (**I**, **J**) and H9C2 cells transfected with siNC or si*Bdh1* (**K**, **L**). **M**, **N** Western blot analysis showing the H3K9 β-hydroxybutyrylation (**M**) and acetylation (**N**) levels in Vehicle- or PA-treated H9C2 cells transfected with Vector- or Flag-BDH1. **O**,**P** Western blot analysis showing the H3K9 β-hydroxybutyrylation and acetylation levels in PA-treated H9C2 cells transfected with siNC- or siBdh1 (**O**) and cardiac tissues from db/m or db/db mice injected with AAV9-Con or AAV9-*Bdh1* (**P**). **Q** Illustration showing the localization of primers on the *Lcn2* promoter. **R**, **S** ChIP assay showing the H3K9bhb enrichment on the *Lcn2* promoter in the PA-treated H9C2 cells transfected with siNC or si*Bdh1* (**R**) and Vector- or Flag-BDH1-transfected H9C2 cells with or without PA treatment (**S**). **T** Illustration showing the BDH1 overexpression-mediated βOHB reduction and the following decreased H3K9bhb on the *Lcn2* promoter. n = 6 mice per group in **A**–**C**. All results are representative of three independent experiments. Values are presented as mean ± SD. **p < 0.05; **p < 0.01; ***p < 0.001*

in H9C2 cells (Fig. 8B–E; Fig. S7A-B). Moreover, ChIP-PCR showed that A485 treatment abolished the palmitic acid-induced elevation of H3K9bhb in promoter region of *Lcn2* (Fig. 8F). Additionally, A485 treatment also activates NF-κB, the downstream of LCN2, but showed no change in BDH1 expression (Fig. S7E-G). We further assessed the effect of A485 on cardiac function through oral administration of A485 to *db/db* mice (Fig. 8G). Compared to *db/m* mice treated with Vehicle, *db/db* mice treated with Vehicle exhibited no changes in systolic function indexes such as EF and FS, the same as that in *db/db* mice treated with A485 (Fig. 8H, I). In contrast, *db/db* mice treated with Vehicle exhibited impaired diastolic function with decreased *E/A* ratio, which was completely reversed by A485 treatment (Fig. 8J,K). Similar to those observed in H9C2 cells, administration of A485 to

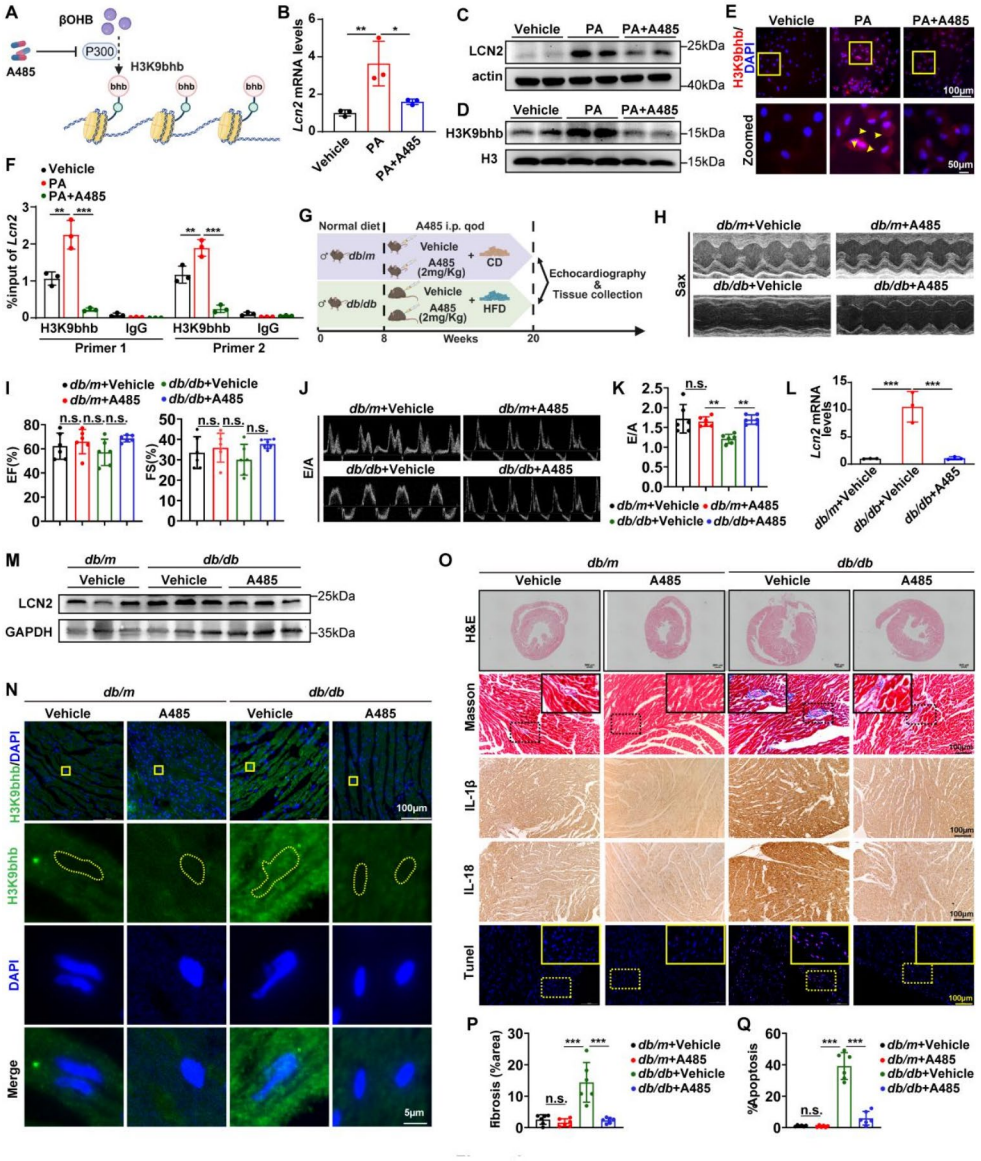

Fig. 8 A485 inhibits the H3K9bhb level of *Lcn2* promoter and attenuates diabetic cardiomyopathy. **A** Illustration showing the inhibition of P300-mediated H3K9bhb by A485. **B**, **C** qRT-PCR and western blot analysis showing the mRNA (**B**) and protein (**C**) levels of LCN2 in H9C2 cells with Vehicle, PA or PA accompanied with A485 treatment. **D**, **E** Representative western blots (**D**) and immunostaining images (**E**) of H3K9bhb in H9C2 cells with Vehicle, PA or PA accompanied with A485 treatment. **F** ChIP analysis showing the H3K9bhb enrichment on the *Lcn2* promoter in H9C2 cells with Vehicle, PA or PA accompanied with A485 treatment. **G** Schematic representation of the animal experiment workflow. **H**, **I** Representative left ventricular M-mode echocardiographic tracings, percentage of left ventricular ejection fraction (EF) and fractional shortening (FS) in the indicated mice. **J**, **K** Representative pulsed-wave Doppler tracings and ratio between mitral E wave and A wave (E/A) in the indicated mice. **L**, **M** qRT-PCR and western blot analysis showing the mRNA (**L**) and protein (**M**) levels of LCN2 in cardiac tissues from *db/m* or *db/db* mice with vehicle or A485 treatment. **N** Representative immunostaining images of H3K9bhb in cardiac tissues from *db/m* or *db/db* mice with vehicle or A485 treatment. **O** Representative images of H&E, Masson staining, immunohistochemistry staining of inflammatory factors and Tunel assay for heart sections from *db/m* or *db/db* mice with vehicle or A485 treatment. Bars: 500 μm in H&E; 100 μm in Masson staining, Tunel assay and immunohistochemistry staining. **P**, **Q** Quantification of fibrosis by assessing the Masson-positive areas (**P**) and apoptosis by counting the Tunel-positive cells (**Q**). n = 6 mice per group. All results are representative of three independent experiments. Values are presented as mean ± SD. **p < 0.05; **p < 0.01; ***p < 0.001*

db/db mice reversed the increase of mRNA and protein levels of LCN2 (Fig. 8L, M; Fig. S7C), as well as the elevation of nuclear H3K9bhb (Fig. 8N). Of note, pathological analysis showed that administration of A485 reversed the diabetes-induced fibrosis, apoptosis and inflammation in *db/db* mice (Fig. 8O, Q; Fig. S7D), which was consistent with that observed in AAV9-*Bdh1* injected *db/db* mice (Fig. 3E). Collectively, these data indicate that BDH1 alleviates DbCM through H3K9bhb-mediated LCN2 transcriptional repression.

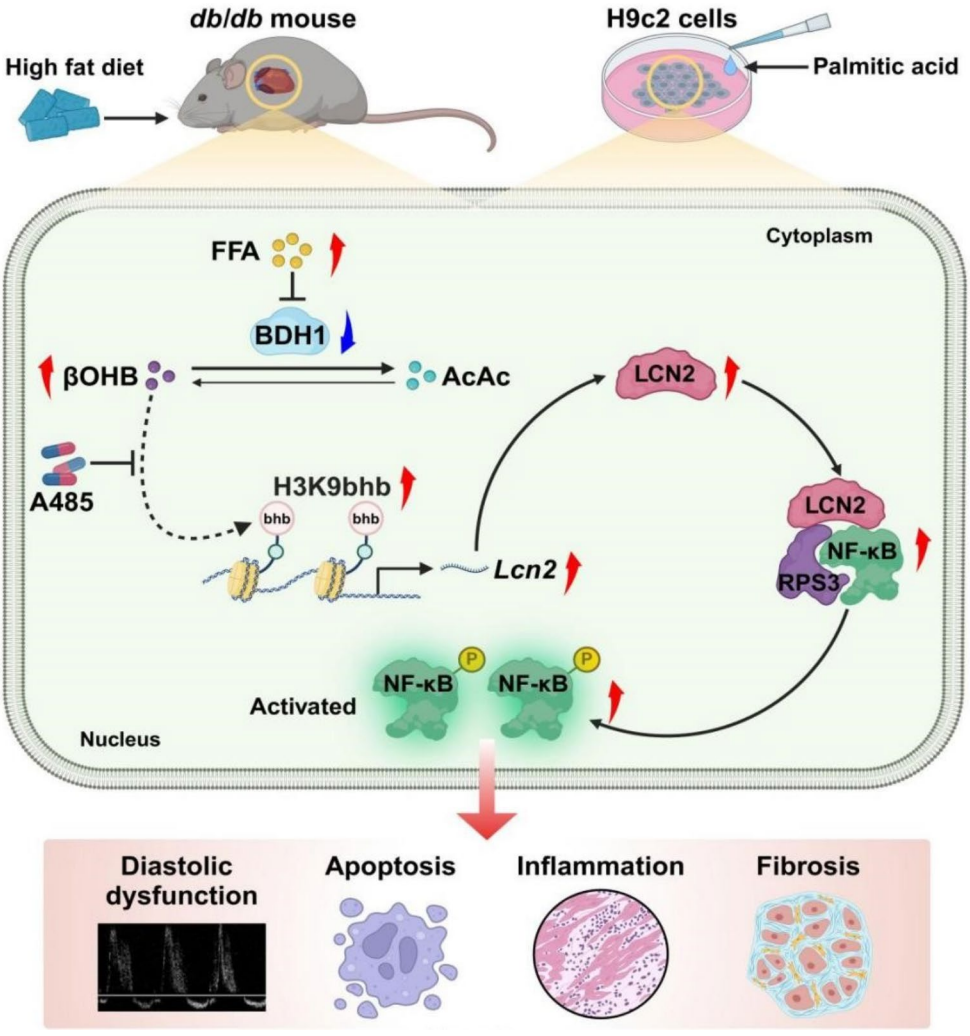

Fig. 9 Schematic diagram depicting the mechanism by which Bdh1-mediated ketone metabolic reprogramming ameliorates DbCM through epigenetic regulation. BDH1 expression is diminished in diabetic hearts in vivo and palmitic acid-treated H9C2 cells in vitro, which leads to ketone metabolic reprogramming characterized by increase of βOHB and the following increased enrichment of H3K9bhb on the Lcn2 promoter. H3K9bhb-mediated Lcn2 transcriptional activation promotes the nuclear localization of NF-κB through enhancing the interaction between NF-κB and RPS3, which finally activates the downstream pathways of inflammation, apoptosis and fibrosis. Illustration created with biorender.com

Discussion

Elevation of ketone bodies, such as ketogenic diet, has been widely reported to ameliorate diabetic complications including DbCM [15, 17]. However, the underlying molecular mechanisms, especially the role of enzymes which mediate the ketone metabolism, in the pathogenesis of DbCM are poorly understood. In this study, we found that BDH1 expression was diminished in cardiac tissues in vivo and palmitic acid-treated H9C2 cells in vitro. BDH1 gain- or loss-of-function studies showed that BDH1 alleviated diabetes-induced cardiac dysfunction, inflammation, apoptosis and fibrosis by inhibiting LCN2/NF-κB signaling through ketone metabolic reprogramming-mediated β-hydroxybutyrylation of H3K9 (Fig. 9). Thus, our study identifies the BDH1-LCN2 axis as a novel targeted signaling in treatment of DbCM.

BDH1-LCN2 axis acts as a novel molecular mechanism in pathogenesis of DbCM

As a rate-limiting enzyme of ketone metabolism [19], BDH1 is reported to be beneficial in various disease. For example, our previous study demonstrated that BDH1 overexpression ameliorates hepatic inflammation, fibrosis and apoptosis via inhibition of oxidative stress in MAFLD mouse model [21]. Besides, cardiac-specific overexpression of BDH1 also mitigates the TAC-induced heart failure through inhibition of oxidative stress [20]. However, the exact roles of BDH1-mediated ketone metabolic reprogramming in diabetic cardiomyopathy are still unknown. Here we identified that BDH1 was remarkably reduced in cardiac tissues of diabetic patients or mouse models (Fig. 1). BDH1 restoration significantly protected against the pathogenesis of DbCM and palmitic

acid-induced lipotoxicity of H9C2 cells (Fig. 3). Interestingly, unlike the previous study in which the BDH1 overexpression functions via repression of oxidative stress, we demonstrated that BDH1 protected against DbCM through negatively regulating LCN2 expression (Figs. 4, 5). LCN2, as an important regulator of inflammation, has been reported to be harmful to metabolic diseases. In diabetic retinopathy, epigenetic silence of *Lcn2* gene by Kdm6a deficiency in macrophages reduces the photoreceptor dysfunction [31]. Chronic infusion of recombinant LCN2 exacerbated diet-induced liver injury and inflammation [32]. Consistently, we observed that LCN2 was prominently increased in diabetic hearts and LCN2 overexpression exacerbated the palmitic acid-induced apoptosis and inflammation in H9C2 cells (Fig. 4). Notably, in this study we identified BDH1 as a new upstream regulator of LCN2 in diabetic hearts. BDH1 knockdown increased, whereas BDH1 overexpression decreased the enrichment of H3K9bhb in the promoter of *Lcn2* (Fig. 7), which was consistent with the changes of mRNA levels (Fig. 4). In a word, we identified BDH1-LCN2 axis as a novel molecular mechanism by which the hyperlipidemia induces cardiomyopathy in T2DM.

BDH1 acts as an epigenetic regulator via metabolic reprogramming

Other than substrates of BDH1, both βOHB and AcAc are also sources of acylation precursors. βOHB could be converted into βOHB-CoA by acetyl CoA synthetase ACSS2 and further acts as substrate of acetyltransferase P300-mediated β-Hydroxybutylation [22]. Acetyl CoA, generated by the metabolism of AcAc, could not only enter the TCA cycle directly, but also undergo histone acetylation under the catalysis of histone acetyltransferases (HATs) [33]. Thus, BDH1-mediated homeostasis of βOHB and AcAc is important for regulation of acylation, including histone-related acetylation and β-hydroxybutylation. In this study, we observed reduction of BDH1 concurrently with increased myocardial βOHB and decreased AcAc as well as the corresponding H3K9bhb and H3K9ac in diabetic condition, which was reversed by BDH1 restoration (Fig. 7), indicating that BDH1 acts as an epigenetic regulator via metabolic reprogramming in DbCM. Notably, as BDH1 is not the only enzyme of ketone metabolism, levels of βOHB and β-hydroxybutylation are also regulated by other limiting enzymes of ketogenesis. In the neonatal heart, 3-hydroxy-3-methylglutaryl-CoA synthase 2 (HMGCS2) is transiently induced by colostrum and promotes βOHB production, which is essential for β-hydroxybutyrylation-mediated mitochondrial maturation [34]. Besides, unlike the BDH1-mediated ketolysis in our study, BDH1 promotes the ketogenesis-generated β-OHB following elevated β-hydroxybutyrylation in CD8+ T-cell memory development [35], which is due to the bi-directional roles of BDH1 in transformation between βOHB and AcAc. Whereas in hepatocellular carcinoma cells and cardiac tissue from a HFpEF mouse model, BDH1 reduction and increased β-OHB or β-hydroxybutyrylation were observed [25, 36], which is consistent with our results. As β-OHB could also function as inhibitor of histone deacetylases (HDACs) or directly binds to cell surface G-protein-coupled receptors (GPCRs) such as hydroxycarboxylic acid receptor 2 (HCAR2) and free fatty acid receptor 3 (FFAR3) [37], whether BDH1-induced reduction of myocardial βOHB participates in pathogenesis of DbCM through these pathways needs further investigation. Anyway, our study revealed that BDH1-mediated ketone metabolic reprogramming ameliorates DbCM via epigenetic regulation.

Cardiac BDH1 restoration is a promising therapy for DbCM due to effective utilization of excessive ketone bodies

As a diet characterized by high fat, moderate protein and low carb, ketogenic diet (KD) was employed by doctors as a treatment for epilepsy as early as the1920s [38]. Thereafter, KD has also been demonstrated to ameliorate diabetes no matter in animal model [39] or patients with T2DM [40], including diabetic complications such as diabetic nephropathy (DN) [41], cardiomyopathy (DbCM) [42] and retinopathy (DR) [43]. KD, as well as the oral administration of βOHB, could steadily increase the blood concentrations of ketone bodies (principally βOHB) in diabetic mouse model, suggesting that the increased blood βOHB is beneficial for reversing of diabetes-induced injury. Whereas in our study, the increased myocardial βOHB led to cell injury via increased H3K9bhb of *Lcn2*, suggesting that the accumulated βOHB in extrahepatic tissues such as heart is not always beneficial. Notably, given that the blood βOHB in diabetic condition is already at a high level, it is reasonable to suppose that promoting the βOHB utilization, but not KD or exogenous ketone supplementation, might also be an effective way in treatment of diabetic complications. In our study, we observed accumulated βOHB in myocardial cells of *db/db* mice and palmitic acid-treated H9C2 cells (Fig. 7) which suggests that the cellular βOHB is sufficient but the βOHB metabolism is deficient because of BDH1 reduction. In view of this, our study provides cardiac BDH1 restoration as a promising therapy for DbCM due to exactly targeting the βOHB metabolism deficiency, which effectively helps cardiomyocytes utilize the excessive βOHB under diabetic condition.

Highlights and limitations

Although several studies were performed to determine the role of BDH1-mediated ketone metabolism in diseases related to heart, kidney or liver, there are several

key points in our study which we think are distinguished from other studies: (1) BDH1 overexpression ameliorates DbCM and palmitic acid-induced lipotoxicity through LCN2/NF-κB signaling pathway. (2) Unlike the always beneficial role of βOHB, here the cardiac βOHB accumulation induced by BDH1 deficiency promoted DbCM by activation of LCN2-mediated inflammatory pathway through H3K9bhb-mediated epigenetic regulation. (3) Cardiac BDH1 restoration or A485-mediated H3K9bhb inhibition effectively alleviates DbCM. However, this study also has limitations. For example, the global knockout of BDH1 would result in hepatic ketone metabolic reprogramming and influence the cardiac levels of βOHB. Moreover, AAV9-mediated BDH1 expression is not limited to cardiac cells but also other cells, especially the hepatic cells which could also induce hepatic ketone metabolic reprogramming and the serum level of βOHB. These would be addressed well if the cardiac-specific deletion or overexpression of BDH1 mouse lines are used in the future study. In addition, the human samples used in this study were collected postmortem rather than from living subjects. This limits their suitability for biochemical assays such as immunohistochemistry, as the results are typically compared to reference intervals established using samples from living individuals. Notably, we collected the original data from studies which performed single cell sequencing [44, 45] or RNA sequencing [46] with heart samples of normal and diabetic patients with heart failure (HF) or HFrEF and found that BDH1 expression was significantly decreased in the cardiomyocytes from diabetes with HF and in the left ventricle from patients with HFrEF (Fig. S8).

Conclusions

In conclusion, here we have revealed a novel molecular mechanism in which the BDH1-LCN2 axis inhibits the pathogenesis of DbCM through ketone metabolic reprogramming-mediated epigenetic regulation. These findings suggest cardiac BDH1 restoration as a promising therapy for DbCM.

Abbreviations

AcAc	Acetoacetate
βOHB	Beta-hydroxybutyrate
BDH1	β-Hydroxybutyrate dehydrogenase 1
ChIP-PCR	Chromatin immunoprecipitation combined real time PCR
DbCM	Diabetic cardiomyopathy
DN	Diabetic nephropathy
DR	Diabetic retinopathy
EF	Ejection fraction
FS	Fractional shortening
FFAR3	Free fatty acid receptor 3
GPCRs	G-protein-coupled receptors
HATs	Histone acetyltransferases
HMGCS2	3-Hydroxy-3-methylglutaryl-CoA synthase 2
HDACs	Histone deacetylases
HCAR2	Hydroxycarboxylic acid receptor 2
HG	High glucose
H&E	Hematoxylin–eosin
HFpEF	Heart failure with preserved ejection
SGLT2i	Inhibitor of sodium-glucose cotransporters 2
IRF7	Interferon regulatory factor 7
IP	Immunoprecipitation
KD	Ketogenic diet
LCN2	Lipocalin 2
PA	Palmitic acid
T2DM	Type 2 diabetes

Supplementary Information

The online version contains supplementary material available at https://doi.org/10.1186/s12933-025-02646-3.

Supplementary Material 1

Acknowledgements

Not applicable.

Author contributions

Z. J., Y. X. and C. Z. designed experiments, analyzed the data, and wrote the manuscript. B. X., S. W., Q. W., Y. X. and Y. H. performed experiments and made figures. W. H. and Y. L. helped with data collection and participated in the manuscript preparation.

Funding

The study was supported by grants from the National Natural Science Foundation of China (No. 82270358; No. U22A20286), the Sichuan Science and Technology Program (No. 2024NSFSC0588) and the Luzhou Science and Technology Program (No. 2023JYJ027).

Availability of data and materials

Data is provided within the manuscript or supplementary information files.

Declarations

Ethics approval and consent to participate

All procedures that involved human samples were approved by the Affiliated Hospital of Southwest Medical University Ethics Committee (KY2023221). Animal experiments were approved by the Institutional Animals Ethics Committees of Southwest Medical University (20220225-014).

Consent for publication

Not applicable.

Competing interests

The authors declare no competing interests.

Author details

[1]Department of Endocrinology and Metabolism, The Affiliated Hospital of Southwest Medical University, Luzhou 646000, Sichuan, People's Republic of China
[2]The People's Hospital of Pingyang, Wenzhou 325000, Zhejiang, People's Republic of China
[3]Metabolic Vascular Disease Key Laboratory of Sichuan Province, Luzhou 646000, Sichuan, People's Republic of China
[4]Experimental Medicine Center, The Affiliated Hospital of Southwest Medical University, Luzhou 646000, Sichuan, People's Republic of China
[5]Sichuan Clinical Research Center for Nephropathy, Luzhou 646000, Sichuan, People's Republic of China
[6]Department of Pathology, and Luzhou Key Laboratory of Precision Pathology Diagnosis for Serious Diseases, The Affiliated Hospital of Southwest Medical University, Luzhou 646000, Sichuan, People's Republic of China
[7]State Key Laboratory of Quality Research in Chinese Medicine, Dr. Neher's Biophysics Laboratory for Innovative Drug Discovery, Faculty of Chinese Medicine, Macau University of Science and Technology, Taipa 999078, Macao, People's Republic of China

[8]Academician (Expert) Workstation of Sichuan Province, The Affiliated Hospital of Southwest Medical University, Luzhou 646000, Sichuan, People's Republic of China

Received: 3 October 2024 / Accepted: 12 February 2025
Published online: 28 February 2025

References

1. Sun H, Saeedi P, Karuranga S, et al. IDF Diabetes Atlas: Global, regional and country-level diabetes prevalence estimates for 2021 and projections for 2045. Diabetes Res Clin Pract. 2022;183:109119.
2. Cavallari I, Bhatt DL, Steg PG, et al. Causes and risk factors for death in diabetes: a competing-risk analysis from the SAVOR-TIMI 53 trial. J Am Coll Cardiol. 2021;77(14):1837–40.
3. Einarson TR, Acs A, Ludwig C, et al. Prevalence of cardiovascular disease in type 2 diabetes: a systematic literature review of scientific evidence from across the world in 2007–2017. Cardiovasc Diabetol. 2018;17(1):1–19.
4. Dillmann WH. Diabetic cardiomyopathy. Circ Res. 2019;124(8):1160–2.
5. Gilbert RE, Krum H. Heart failure in diabetes: effects of anti-hyperglycaemic drug therapy. The Lancet. 2015;385(9982):2107–17.
6. ACCORD Study Group. Nine-year effects of 37 years of intensive glycemic control on cardiovascular outcomes. Diabetes Care. 2016;39(5):701–8.
7. Puchalska P, Crawford PA. Multi-dimensional roles of ketone bodies in fuel metabolism, signaling, and therapeutics. Cell Metab. 2017;25(2):262–84.
8. Abdul Kadir A, Clarke K, Evans RD. Cardiac ketone body metabolism. Biochim Biophys Acta Mol Basis Dis. 2020;1866(6):165739.
9. Ferrannini E, Baldi S, Frascerra S, et al. Shift to fatty substrate utilization in response to sodium-glucose cotransporter 2 inhibition in subjects without diabetes and patients with type 2 diabetes. Diabetes. 2016;65(5):1190–5.
10. Suzuki M, Takeda M, Kito A, et al. Tofogliflozin, a sodium/glucose cotransporter 2 inhibitor, attenuates body weight gain and fat accumulation in diabetic and obese animal models. Nutr Diabetes. 2014;4(7):e125.
11. Mudaliar S, Alloju S, Henry RR. Can a shift in fuel energetics explain the beneficial cardiorenal outcomes in the EMPA-REG OUTCOME study? A unifying hypothesis. Diabetes Care. 2016;39(7):1115–22.
12. Zinman B, Wanner C, Lachin JM, et al. Empagliflozin, cardiovascular outcomes, and mortality in type 2 diabetes. N Engl J Med. 2015;373(22):2117–28.
13. Fang Y, Chen B, Gong AY, et al. The ketone body β-hydroxybutyrate mitigates the senescence response of glomerular podocytes to diabetic insults. Kidney Int. 2021;100(5):1037–53.
14. Bai L, Zhou Y, Zhang J, et al. The role of a ketogenic diet in the treatment of dementia in type 2 diabetes mellitus. Nutrients. 2023;15(8):1971.
15. Trang NN, Lee T-W, Kao Y-H, et al. Ketogenic diet modulates cardiac metabolic dysregulation in streptozocin-induced diabetic rats. J Nutr Biochem. 2023;111:109161.
16. Møller N. Ketone body, 3-hydroxybutyrate: minor metabolite—major medical manifestations. J Clin Endocrinol Metab. 2020;105(9):2884–92.
17. Suxin L, Xia Y, Zhai Q, et al. Ketogenic diet ameliorates cardiac dysfunction via balancing mitochondrial dynamics and inhibiting apoptosis in type 2 diabetic mice. Aging Disease. 2020;11(2):229.
18. Abdurrachim D, Teo XQ, Woo CC, et al. Cardiac metabolic modulation upon low-carbohydrate low-protein ketogenic diet in diabetic rats studied in vivo using hyperpolarized13C pyruvate, butyrate and acetoacetate probes. Diabetes Obes Metab. 2019;21(4):949–60.
19. Otsuka H, Kimura T, Ago Y, et al. Deficiency of 3-hydroxybutyrate dehydrogenase (BDH1) in mice causes low ketone body levels and fatty liver during fasting. J Inherit Metab Dis. 2020;43(5):960–8.
20. Uchihashi M, Hoshino A, Okawa Y, et al. Cardiac-specific Bdh1 overexpression ameliorates oxidative stress and cardiac remodeling in pressure overload–induced heart failure. Circ Heart Fail. 2017;10(12):e004417.
21. Xu B, Teng F, Wu Q, et al. Bdh1 overexpression ameliorates hepatic injury by activation of Nrf2 in a MAFLD mouse model. Cell Death Discov. 2022;8(1):49.
22. Xie Z, Zhang D, Chung D, et al. Metabolic regulation of gene expression by histone lysine β-hydroxybutyrylation. Mol Cell. 2016;62(2):194–206.
23. Wu X, Miao D, Liu Z, et al. β-hydroxybutyrate antagonizes aortic endothelial injury by promoting generation of VEGF in diabetic rats. Tissue Cell. 2020;64:101345.
24. Luo W, Yu Y, Wang H, et al. Up-regulation of MMP-2 by histone H3K9 β-hydroxybutyrylation to antagonize glomerulosclerosis in diabetic rat. Acta Diabetol. 2020;57(12):1501–9.
25. Zhang H, Chang Z, Qin L, et al. MTA2 triggered R-loop trans-regulates BDH1-mediated β-hydroxybutyrylation and potentiates propagation of hepatocellular carcinoma stem cells. Signal Transduct Target Ther. 2021;6(1):135.
26. Ma X-M, Geng K, Law BY, et al. Lipotoxicity-induced mtDNA release promotes diabetic cardiomyopathy by activating the cGAS-STING pathway in obesity-related diabetes. Cell Biol Toxicol. 2023;39(1):277–99.
27. Wang X, Zhang R, Zhang S, et al. Interferon regulatory factor 7 deficiency prevents diet-induced obesity and insulin resistance. Am J Physiol Endocrinol Metab. 2013;305(4):E485-495.
28. Jang HM, Lee JY, An HS, Ahn YJ, Jeong EA, Shin HJ, et al. LCN2 deficiency ameliorates doxorubicin-induced cardiomyopathy in mice. Biochem Biophys Res Commun. 2022;588:8–14.
29. Huang Z, Zhang Y, Li H, et al. Vitamin D promotes the cisplatin sensitivity of oral squamous cell carcinoma by inhibiting LCN2-modulated NF-kappaB pathway activation through RPS3. Cell Death Dis. 2019;10(12):936.
30. Wu S, Zhou Y, Liang J, et al. Upregulation of NF-kappaB by USP24 aggravates ferroptosis in diabetic cardiomyopathy. Free Radic Biol Med. 2024;210:352–66.
31. Wen Y, Chen X, Feng H, et al. Kdm6a deficiency in microglia/macrophages epigenetically silences Lcn2 expression and reduces photoreceptor dysfunction in diabetic retinopathy. Metabolism. 2022;136:155293.
32. Ye D, Yang K, Zang S, et al. Lipocalin-2 mediates non-alcoholic steatohepatitis by promoting neutrophil-macrophage crosstalk via the induction of CXCR2. J Hepatol. 2016;65(5):988–97.
33. Liu Y, Vandekeere A, Xu M, et al. Metabolite-derived protein modifications modulating oncogenic signaling. Front Oncol. 2022;12:988626.
34. Arima Y, Nakagawa Y, Takeo T, et al. Murine neonatal ketogenesis preserves mitochondrial energetics by preventing protein hyperacetylation. Nat Metab. 2021;3(2):196–210.
35. Zhang H, Tang K, Ma J, et al. Ketogenesis-generated beta-hydroxybutyrate is an epigenetic regulator of CD8(+) T-cell memory development. Nat Cell Biol. 2020;22(1):18–25.
36. Deng Y, Xie M, Li Q, et al. Targeting mitochondria-inflammation circuit by beta-hydroxybutyrate mitigates HFpEF. Circ Res. 2021;128(2):232–45.
37. Newman JC, Verdin E. Beta-hydroxybutyrate: a signaling metabolite. Annu Rev Nutr. 2017;37:51–76.
38. Brietzke E, Mansur R, Subramaniapillai M, et al. Ketogenic diet as a metabolic therapy for mood disorders: Evidence and developments. Neurosci Biobehav Rev. 2018;94:11–6.
39. Geng S, Zhu W, Xie C, et al. Medium-chain triglyceride ameliorates insulin resistance and inflammation in high fat diet-induced obese mice. Eur J Nutr. 2016;55:931–40.
40. Takeuchi H, Noguchi O, Sekine S, et al. Lower weight gain and higher expression and blood levels of adiponectin in rats fed medium-chain TAG compared with long-chain TAG. Lipids. 2006;41:207–12.
41. Poplawski MM, Mastaitis JW, Isoda F, et al. Reversal of diabetic nephropathy by a ketogenic diet. PLoS ONE. 2011;6(4):e18604.
42. Guo Y, Zhang C, Shang FF, et al. Ketogenic diet ameliorates cardiac dysfunction via balancing mitochondrial dynamics and inhibiting apoptosis in type 2 diabetic mice. Aging Dis. 2020;11(2):229–40.
43. Chandrasekaran P, Rani PK. Reversal of diabetic tractional retinal detachment attributed to keto diet. BMJ Case Rep. 2020;13(10):e235873.
44. Koenig AL, Shchukina I, Amrute J, et al. Single-cell transcriptomics reveals cell-type-specific diversification in human heart failure. Nat Cardiovasc Res. 2022;1(3):263–80.
45. Amrute JM, Lai L, Ma P, et al. Defining cardiac functional recovery in end-stage heart failure at single-cell resolution. Nat Cardiovasc Res. 2023;2(4):399–416.
46. Luo X, Yin J, Dwyer D, et al. Chamber-enriched gene expression profiles in failing human hearts with reduced ejection fraction. Sci Rep. 2021;11(1):11839.

Publisher's Note